ADVANCES IN ATMOSPHERIC SCIENCES, VOL. 25, NO. 4, 2008, 541–554

The Wavenumber-Frequency Characteristics of the Tropical Waves in an Aqua-Planet GCM

WANG Zaizhi[1,2] (王在志), MAO Jiangyu[1] (毛江玉), and WU Guoxiong[*1] (吴国雄)

[1]*State Key Laboratory of Numerical Modeling for Atmospheric Sciences and Geophysical Fluid Dynamics (LASG), Institute of Atmospheric Physics, Chinese Academy of Sciences, Beijing* 100029

[2]*National Climate Center, China Meteorological Administration, Beijing* 100081

(Received 16 May 2007; revised 7 April 2008)

ABSTRACT

Based on the aqua-planet experiments, the wavenumber-frequency characteristics of tropical waves and their influencing factors in SST distribution and the convective parameterization scheme are investigated using the spectral atmospheric general circulation model (SAMIL). Space-time spectral analysis is used to obtain the variance of convectively coupled tropical waves. In the Control experiment with maximum SST located at the equator the simulated tropical-wave behaviors are in agreement with those in observations and theoretical solutions. When the maximum SST is located at 5°N, the symmetric and antisymmetric waves are much weaker than those in the control experiment, suggesting that tropical wave activities are very sensitive to the SST distributions. Importantly, the variance maximum of Madden-Julian oscillation (MJO) is found to occur around 5°N, which suggests that the development of the MJO depends largely on the latitude of maximum SST. Furthermore, the seasonal variations of MJO may be mainly caused by the seasonal variations of the maximum SST.

The experiment results with two different cumulus schemes—the Manabe moist convective adjustment and Zhang-McFarlane (ZM) convective scheme, were also compared to examine the impacts of convective parameterization. Weakened variances of each individual tropical wave when the ZM scheme is used suggest that the ZM scheme is not favorable for the tropical wave activities. However, the wave characteristics are different when the ZM scheme is used in different models, which may imply that the simulated basic state is important to the meridional distributions of the waves. The MJO signals suggest that the parameterization scheme may have great influence on the strength, but have less direct impact on the MJO distribution. The frequency of the tropical waves may be associated with the moisture control of convection and the large-scale condensation scheme used in the model.

Key words: tropical wave, SAMIL, convective processes

DOI: 10.1007/s00376-008-0541-3

1. Introduction

Tropical atmospheric waves are induced mostly by convective heating in the troposphere, and are related to the interactions between internal atmospheric dynamics and external forcing (Lau and Peng, 1987; Yang et al., 2003). With the development of satellite observation, some new phenomena and facts were found in the tropics such as Madden-Julian oscillations (MJO; Madden and Julian, 1971, 1994). Madden and Julian (1994) summarized the structure and propagation of the MJO as well as its possible formation mechanism. Based on satellite data with high spatial-temporal resolution, the wave spectra of other tropical waves with different frequencies were also examined (e.g., Wheeler and Kiladis, 1999; Ichikawa and Yasunari, 2006). Although some theoretical studies have been made to explain the basic features of these tropical waves, until now there has been a limited knowledge of their structure, propagation, and origin.

An atmospheric general circulation model (AGCM), or coupled ocean-atmosphere model, is a useful tool for investigating the processes that deter-

*Corresponding author: WU Guoxiong, gxwu@lasg.iap.ac.cn

mine the characteristics of the tropical waves. AGCM has been widely used in studies of intraseasonal oscillation activities and their impacts, especially the MJO simulations due to its importance in the climate system (e.g., Swinbank et al., 1988; Li et al., 2006; Dong et al., 2006). Based on AGCM simulations, not only the propagation features of the tropical waves associated with sea surface state, but also the influences of different physical processes and air-sea interactions on these waves, can be recognized (Maloney and Hartmann, 2001; Liu et al., 2005). In addition to the MJO, other tropical convectively coupled waves, such as the equatorial Rossby waves and the inertio-gravity waves, also strongly affect tropical weather. However, complex interactions exist in AGCMs, which make it difficult to analyze the impact mechanism of tropical waves. Moreover, uncertainties are present in simulated results from different models. To probe the reasons for the differences in the systematic errors of each of the models, the Atmospheric Model Intercomparison Project (AMIP) has been implemented in recent years (Gates, 1992). In an evaluation of 15 AGCMs as part of the AMIP, Slingo et al. (1996) indicated the typical shortcomings of too-weak intensity and too-fast propagation of the intraseasonal oscillations in the modeling. Recently Lin (2006) evaluated the tropical intraseasonal variability with 14 coupled GCMs participating in the Intergovernmental Panel on Climate Change (IPCC) Fourth Assessment Report (AR4). Their results showed that AGCMs have significant problems but display a wide range of skill in simulating the tropical intraseasonal variability.

In view of the complexity of the spatial and temporal variability of boundary conditions such as the land/sea distribution, orography, and SST forcing, it is more difficult to understand their interactions (Neale and Hoskins, 2001a). Simplified models were used to simulate the mechanism responsible for the frequency and propagation of tropical waves (e.g., Lau and Peng, 1987; Yang et al., 1990; Raymond, 2001), which can provide additional suggestions for the improvement of GCM simulations of tropical intraseasonal variability. Therefore, some simplified projects were proposed using idealized GCMs that can bridge the gap between simple models and full GCMs, such as the intercomparison project to compare the dynamical cores of AGCMs based on a simplified approach proposed by Held and Suarez (1994). The aqua-planet (AP) experiment project was proposed to test the interaction of the physical parameterizations in an AGCM with each other and with the dynamics (Neale and Hoskins, 2001a), in which the full AGCM is retained but the surface boundary is drastically simplified as only ocean without land. For a set of AP experiments designed to test how AGCMs respond to different characteristics of SST forcing, all models are required to use identical prescribed and very idealized SST distributions. Based on the comparison of the outputs from different AGCMs under controlled conditions, one can understand the model performances, the reasons for differences in different models, and the impacts of different physical parameterizations, etc. Since it rules out topographic or thermal land-sea contrast effects, such differences demonstrate the usefulness of AP experiments in emphasizing model differences which are difficult to identify when complex observed boundary forcing is included.

Actually, before the AP experiment project was proposed, similar experiments with AGCMs had been carried out to study some tropical phenomena involving the MJO, ITCZ, and the Hadley circulation (Swinbank et al., 1988; Numaguti, 1995). Similar simulations were also implemented to investigate the impacts of the SST anomaly in the Indian Ocean on the subtropical anticyclone over the western Pacific via two-stage thermal adaptation in the atmosphere (Wu et al., 2002). Hess et al. (1993) performed a suite of AP experiments integrated with identical SSTs, but with two different convective parameterization schemes, and their results showed that two distinctly different tropical ITCZ regimes occurred purely in response to the two different schemes used. Lee et al. (2003) found that simulated tropical intraseasonal oscillations are largely sensitive to convection scheme, and that schemes in which it is more difficult to convect tend to produce stronger variability. Frierson (2007) studied the dependence of Kelvin waves on quantities such as the gross moist stability with a zonally symmetric aqua-planet and slab mixed layer ocean boundary conditions.

The main objective of this study is to explore the behaviors of tropical wave activities as well as the impacts of different SST distributions and different convective parameterization schemes on these waves by examining the simulated results in an AGCM. A set of AP experiments are conducted, because it is more useful for interpreting the different response of the model due to the change of the cumulus scheme, and investigating the interaction between model dynamics and physical parameterizations.

The model description and experiment setup in this study are briefly presented in section 2. The theoretical backgrounds for tropical waves and methodology for wavenumber-frequency filtering are introduced in section 3. Analyses of the experiment results are detailed in sections 4, 5 and 6. The conclusions and discussions are given in section 7.

2. Model description and experiment setup

2.1 *Model description*

The model used in this study is a spectral AGCM (named SAMIL), which is the atmospheric component of the flexible global ocean-atmosphere-land system (FGOALS) developed by the State Key Laboratory of Atmospheric Sciences and Geophysical Fluid Dynamics/Institute of Atmospheric Physics (LASG/IAP). Its dynamic framework includes the "standard atmosphere subtraction" scheme (Wu et al., 1996) in which a time independent standard atmosphere is introduced and subtracted to reduce the calculation errors of the pressure gradient force. The resolution of SAMIL model is flexible, and two optional dynamical frameworks in σ-coordinate and in η-coordinate systems are designed, while multiple schemes with corresponding physical processes are provided and can be conveniently selected for comparison studies. In the present study, the dynamical framework adopted is the σ-coordinate system with 9 vertical layers, and rhomboidally truncated at wavenumber 42 in the horizontal (R42, a roughly 2.8125° lon ×1.66° lat Gaussian grid) (Wang et al., 2004). Also included are a K-distribution radiation scheme that was originally developed by Shi (1981) with the diurnal variation (Shao et al., 1998), and Slingo's cloud diagnosis scheme (Slingo, 1987) that depends on relative humidity and vertical velocity. The convection process is handled with the Manabe moist adjustment scheme (Manabe et al., 1965). Turbulent fluxes are given by the vertical diffusion scheme of Louis (1979) based on Monin-Obukov similarity theory. A detailed description of the model can be found in Zhang et al. (2000) and Wang et al. (2004). The SAMIL model has succeeded in simulating rainfall patterns over the Tropics and East Asia and their seasonal changes (Wang et al., 2004), but it is unable to effectively simulate tropical intraseasonal oscillations (Li et al., 2006) as in other GCMs (Slingo et al., 1996).

2.2 *Experiment setup*

According to the AP project experiment design, the boundary conditions are assumed to be zonally symmetric SST distributions varying in latitude only, and the form of the SST distributions are specified by simple smooth geometric functions (Neale and Hoskins, 2001a). Here, two experiments are first performed to examine the influence of the SST distributions on tropical convectively coupled waves. One is called the Control experiment in which the maximum SST is located at the equator. The SST variations are as following.

$$T_{\rm s}(\lambda,\varphi)=\begin{cases} 27\left[1-\sin^2\left(\dfrac{3\varphi}{2}\right)\right], & -\dfrac{\pi}{3}<\varphi<\dfrac{\pi}{3} \\ 0, & \text{otherwise} \end{cases} \tag{1}$$

where $T_{\rm s}(\lambda,\varphi)$ denotes the SST, λ is longitude, and φ is latitude.

Another experiment is referred to as the Control-5N experiment in which maximum SSTs are set at 5°N with the meridional SST distribution subject to formula (2). Such a SST distribution is the only difference from the Control experiment, which can be used to reflect the seasonal variations in the real world.

$$T_{\rm s}(\lambda,\varphi)= \begin{cases} 27\left\{1-\sin^2\left[\dfrac{90}{55}\left(\varphi-\dfrac{\pi}{36}\right)\right]\right\}, & \dfrac{\pi}{36}\leqslant\varphi<\dfrac{\pi}{3} \\ 27\left\{1-\sin^2\left[\dfrac{90}{65}\left(\varphi-\dfrac{\pi}{36}\right)\right]\right\}, & -\dfrac{\pi}{36}<\varphi<\dfrac{\pi}{36} \\ 0, & \text{otherwise} \end{cases} \tag{2}$$

To understand the impacts of other physical processes and dynamical framework on the tropical waves, the results of the Community Atmosphere Model (NCAR CCSM CAM2), provided by the aqua-planet experiment (APE) Project (hereafter NCAR-Control), are analyzed in this study, in which the same controlled conditions are used as in Control experiment.

To compare the influences of different convective parameterization schemes on tropical waves, the Zhang-McFarlane convective scheme (ZM, Zhang and McFarlane, 1995) of the NCAR CCM3 model is introduced into the SAMIL model. Then a similar experiment is performed with the same SST distributions used in the Control experiment (hereafter called Control-ZM). As compared with the Control experiment results, one can realize the influence of convective parameterization scheme on the tropical waves.

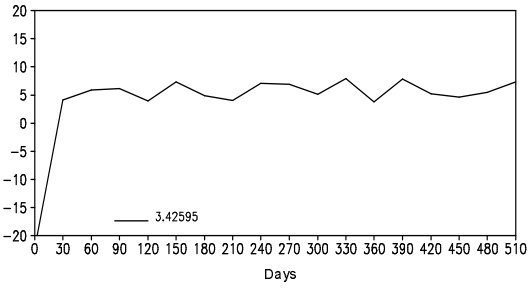

Fig. 1. The time evolution of atmospheric energy budget (W m^{-2}) in the Control experiment.

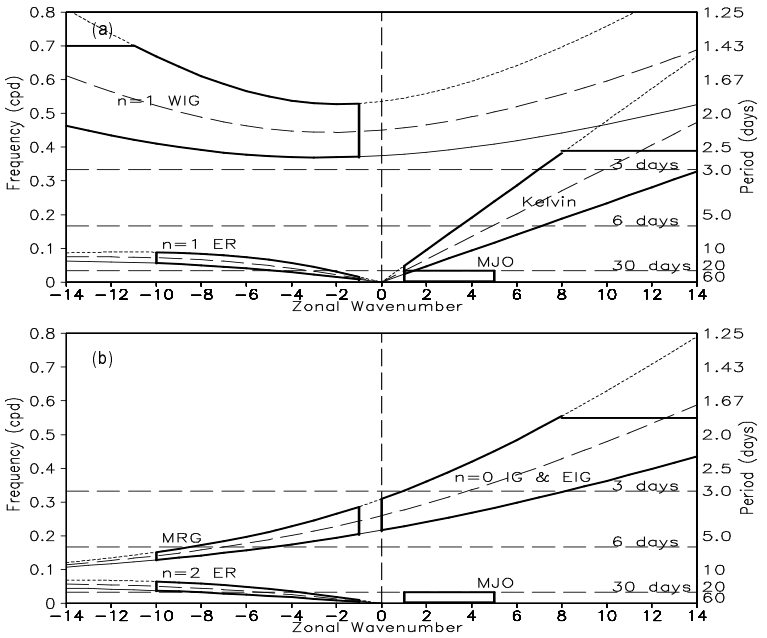

Fig. 2. Theoretical dispersion curves of tropical waves. Thin lines are the various tropical wave dispersion curves for the different equivalent depths of 12 m (solid), 25 m (dashed), and 50 m (dotted). Thick boxes denote the interest regions of wavenumber-frequency domain used to filter the typical waves including Kelvin, ER, MRG, WIG, EIG, and MJO waves (see text for details) for the (a) symmetric and (b) antisymmetric components of the simulated precipitation.

The above AP experiments are initialized using model restarts from the full AGCM interpolated to zero orography. In each experiment the model integrates for 18 months, with the first 6 months taken as the adjustment period. The results from the last 12 months are examined for this study, with analyses of tropical waves based on 6-hourly precipitation within the last 360 days.

During the model integration for each of the AP experiments, besides the SST forcing prescribed, the insolation is also fixed at March equinoctial conditions to make the radiation forcings symmetric about the equator. Thus the model run can reach an equilibrium state quickly. The temporal variations of the simulated global-mean net energy absorbed by the atmosphere in the Control experiment are shown in Fig. 1. The adjustment period of the model run is found within the initial 60 days. Subsequent small and steady variations are consistent with the external forcings.

3. Tropical wave theory and wavenumber-frequency filtering

Convectively coupled tropical waves have been studied theoretically and observationally for several decades (e.g., Matsuno, 1966; Lindzen, 1967; Gill, 1980; Wheeler and Kiladis, 1999; Yang et al., 2003). Theoretically, tropical wave solutions of the shallow water equations are characterized by four parameters involving meridional mode number n, frequency, planetary zonal wavenumber, and equivalent depth of the shallow layer of fluid. Based on the wavenumber and/or frequency, tropical waves can be classified into equatorial Rossby (ER), mixed Rossby-gravity (MRG), eastward inertio-gravity (EIG), westward inertio-gravity (WIG), and Kelvin waves (Fig. 2). Note that each of these tropical waves is either antisymmetric or symmetric about the equator (Wheeler and Kiladis, 1999). In practice, various methods have been developed to identify the structures of tropical waves from observational data. Yang et al. (2003) proposed a new methodology to detect wave structures by projecting upper and lower tropospheric data onto tropical wave modes. Based on satellite-observed outgoing longwave radiation (OLR), Wheeler and Kiladis (1999) used a space-time spectral analysis to isolate the convective variations contributing to spectral peaks, which coincide with the equatorial wave dispersion curves for various equivalent depths. Their study suggested that a portion of the space-time variability of deep tropical cloudiness inferred from OLR could be described quite well in terms of equatorially trapped

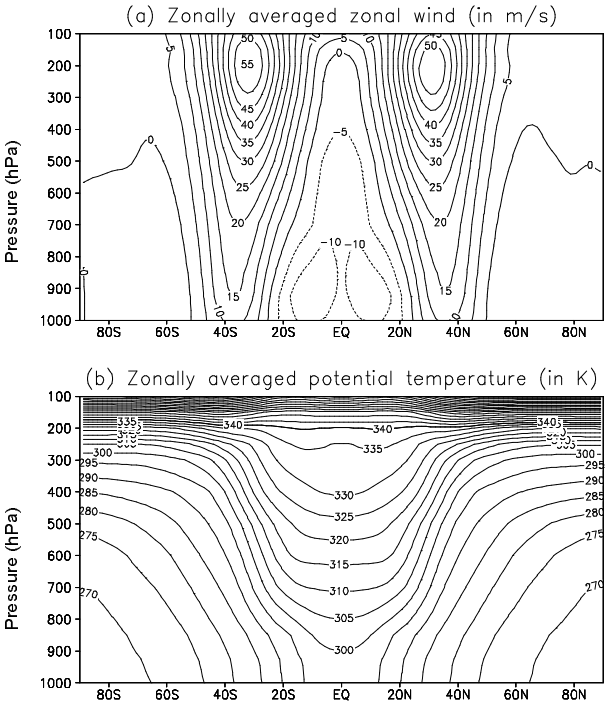

Fig. 3. Pressure-latitude cross sections of (a) zonal-mean zonal wind (m s^{-1}) and (b) zonal-mean potential temperature (K) in the Control experiment.

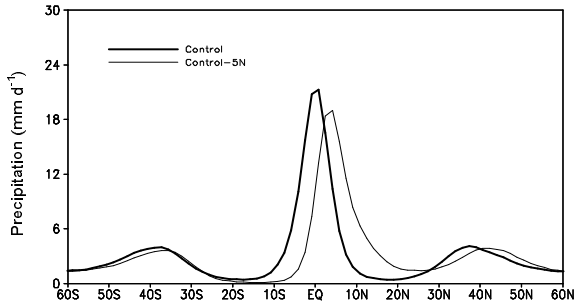

Fig. 4. Zonal-mean precipitation (mm d^{-1}) for the Control (thick line) and Control-5N (thin line) experiments.

wave modes from shallow water theory. As an important component within tropical waves, the MJO is also detected in the OLR spectra, although it does not correspond to any of the theoretical equatorially trapped wave dispersion curves. These suggest that such a space-time spectral technique is particularly useful for identifying the characteristics of tropical waves (Hayashi, 1982). Therefore, this technique is used in this research based on the simulated total precipitation. As stated above, the simulated precipitation rate during the model days 181–540 are used to perform the space-time spectrum analysis. The precipitation power is averaged between 10°S and 10°N.

Following Wheeler and Kiladis (1999), in this study the behaviors of some tropical waves are also explored by filtering in the wavenumber-frequency domain. Here the "regions of interest" waves in the wavenumber-frequency domain are specified according to the theoretical dispersion relation, and are shown in Fig. 2. The wavenumber-frequency filtering of the simulated precipitation is thus performed by taking the inverse of the space-time transform processes only with those Fourier coefficients that are within the specified "region of interest" waves in the wavenumber-frequency domain.

4. The Control experiment results

4.1 *Zonal mean states*

As the SST and other external forcings are zonally distributed in the AP experiment, the zonal-mean states are shown here to see if the results are reasonable. The simulated zonally-averaged zonal wind and potential temperature from the Control experiment are illustrated in Fig. 3. Strong easterlies are present in the lower tropical troposphere, with the westerly jet stream in the mid-latitudinal upper troposphere in each hemisphere (Fig. 3a). Both zonal wind and temperature exhibit a symmetric distribution about the equator due to symmetric SST and radiation distributions in the meridional direction. Although the circulation patterns are simpler than those in real atmosphere, the distributions of the simulated circulation systems are reasonable. Notice that the westerly zone is confined to a relatively narrow extent, which may result from reduced or weak stationary eddy transport, and further due to no land-sea thermal contrast and topography (Swinbank et al., 1988). Correspondingly, meridional temperature gradients in the midlatitudes are larger than those in the real atmosphere (Fig. 3b), leading to the westerlies being too strong there. In the tropics the temperature is higher than that in the actual state, which may be caused by enhanced diabatic heating. Note that stronger than observed precipitation occurs in the equatorial region (see Fig. 4). Similar situations appeared in the simulated results given by Neale and Hoskins (2001b), who used the HadAM3 model to perform the AP experiments.

Figure 4 shows the simulated zonal mean precipitation from the Control and Control-5N experiments. For the Control results, precipitation maxima occur around the equator due to maximum SSTs, and the value is about 20 mm d^{-1}, which is almost twice as much as that in the real world. The width and strength of strong precipitation appear to depend largely on the meridional SST gradient though the maximum SSTs are the same. In another experiment in which the SST

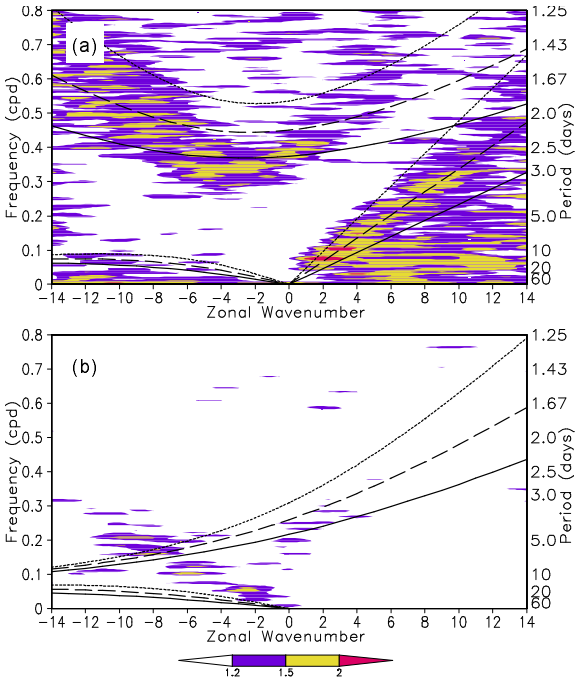

Fig. 5. The power spectrum ratios (shading) of tropical waves to the background power in the wavenumber-frequency domain in the Control experiment for (a) Symmetric component, and (b) Antisymmetric component. Superimposed are the theoretical dispersion curves for several equivalent depths of 12 m (solid), 25 m (dashed), and 50 m (dotted). The wavenumber-frequency power spectrum is based on the simulated total precipitation averaged between 10°S and 10°N.

gradient is flattened (not shown), the rainfall at the equator is reduced and two peaks occur on the north and south sides of the equator, representing the double ITCZ. Additionally, a second maximum of precipitation also exists in the midlatitudes of each hemisphere. These simulation features are qualitatively similar to the observed climatology of the annual-mean precipitation.

4.2 *Wavenumber-frequency characteristics of tropical waves*

Figure 5 displays the power spectrum ratios of tropical waves to the total power in the wavenumber-frequency domain for the Control experiment, in which the theoretical dispersion curves for several equivalent depths are superimposed for comparison. The eastward propagating Kelvin wave and the WIG are found to be the dominant symmetric waves (Fig. 5a). Each of these two waves is consistent with theoretical dispersion relation and accounts for a significant amount of variability. With an equivalent depth around 25 m, this is remarkably similar to the observation (Lin, 2006). The $n = 1$ ER wave can be also identified in Fig. 5a where n is the meridional mode number of the wave. The antisymmetric waves mainly include the MRG and $n = 2$ ER waves (Fig. 5b) and these waves are also observed in the real atmosphere (Wheeler and Kiladis, 1999). Although the simulated MJO is not significant for wavenumbers 1–2, it is significant for wavenumbers 4–10 (Fig. 5a). Actually, the wave disturbances with the period of greater than 30 days simulated by other AP experiments are also very weak (e.g., Swinbank et al., 1988; Neale and Hoskins, 2001b). Based on the AMIP studies, Slingo et al. (1996) also found that several models tend to capture intraseasonal oscillations, and nearly all models have relatively more power at higher frequencies (<30 days) than in observations, but underestimate the strength of the intraseasonal variability. The above results indicate such errors may be associated with the AGCM physical parameterizations. These errors may also result from the SST prescribing that the models are unable to sufficiently deal with the realistic air-sea interaction processes. In the AP and AMIP experiments, for instance, the SST distributions are all prescribed, thus the air-sea interaction processes are also simplified. Using a coupled ocean-atmosphere model, Waliser et al. (1999) conducted a set of simulating experiments to examine the influence of coupled SSTs

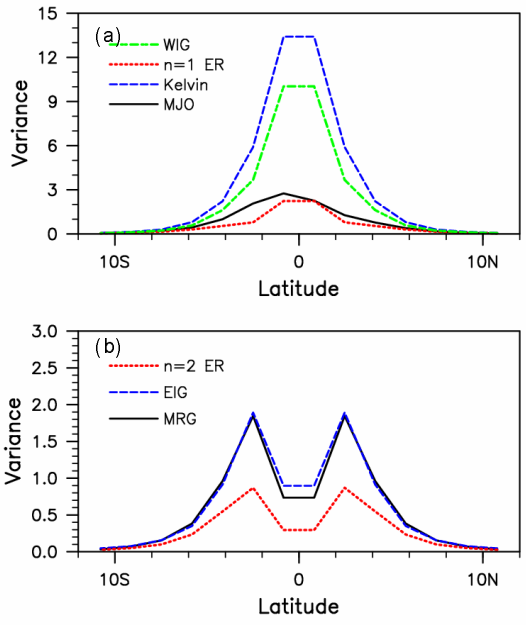

Fig. 6. Zonal-mean variances of simulated precipitation for various parts of the wavenumber-frequency domain of interest for the Control experiment. (a) Symmetric waves, (b) Antisymmetric waves. The variance values have been scaled by 10^{-9} (kg m^{-2} s^{-1})^2.

on MJO. In the "coupled" simulation, the model is coupled to a slab ocean mixed layer that provides prognostic SST anomalies. The results showed that the simplified air-sea interactions facilitate a better simulation with respect to a number of general model shortcomings associated with the MJO that were documented by Slingo et al. (1996) in the AMIP study. Furthermore, the simulated MJO is also stronger and more realistic as it is forced by weekly SSTs than by monthly SSTs (Li et al., 2002).

The tropical wave features are further examined by filtering in the wavenumber-frequency domain, with the "regions of interest" waves of the wavenumber-frequency domain defined in Fig. 2. The variance for all scales from planetary to synoptic waves shows that the maximum variance occur over the equatorial region, with some main centers at different longitudes (not shown), which suggests that zonally symmetric SST and radiation distributions can induce some organized convective centers. However, since the SST and other external forcings are zonally distributed, the geographical domain may have no special meanings. Figure 6 displays the zonal mean distributions of simulated precipitation variances from the Control experiment for each wavenumber-frequency bands. The Kelvin wave is the most significant among these waves (Fig. 6a) with its variance explaining more than 10% of the variance of all the scale waves in the tropics, and is more confined to the equator. The WIG wave has the variance of a slightly smaller magnitude compared to the Kelvin wave. The variance of MJO is weak and is comparable to that of $n = 1$ ER wave, which is not consistent with observational studies (e.g., Wheeler and Kiladis, 1999) that the MJO is the strongest than the Kelvin wave, but is consistent with other GCMs (Slingo et al., 1996). Note that the maximum variance of the symmetric waves occurs over the equator, while the maximum variance of antisymmetric components is away from the equator and also weaker (Fig. 6b). The $n = 2$ ER wave is the weakest, which explains the least amount of precipitation variance of all of the wave modes isolated in the present study. The MRG and EIG waves have the similar variance magnitudes, which is also shown in the observational study that the MRG variance should be comparable to those of the EIG waves (Wheeler and Kiladis, 1999). So, the results of AP experiment can represent those from AMIP and compare with the observations.

As done by Wheeler and Kiladis (1999), the propagation features of tropical waves can be identified based on the time-longitude realizations. Figure 7 shows the time-longitude cross sections of the precipitation anomalies averaged between 10°S and 10°N. The signals of the $n = 1$ ER waves are found to propagate significantly westward with a phase speed of about 4 m s^{-1}, while the Kelvin wave moves eastward at a quicker speed of around 15 m s^{-1} and propagates almost globally. The WIG wave is much faster with a phase speed of about 20 m s^{-1} and can be seen to have much more widely varying time and space scales. Because of a smaller amplitude variance in the MJO band (Fig. 6), the MJO signal shown here is also weak with the same amplitude of $n = 1$ ER wave. Its eastward propagation appears to exist with the zonal wave number around 4.

5. Response to the off-equatorial maximum SST forcing

Since the influences of land-sea thermal contrast and orography have been removed in both the Control and Control-5N experiment, these simulated results can reflect the tropical atmospheric response to different characteristics of SST forcing. In the Control-5N experiment, the maximum rainfall (Fig. 4) moves away from the equator due to off-equatorial maximum SSTs, exhibiting a broader maximum extent than in the Control experiment. Although the SST maxima in both experiments are 27°C, the precipitation maximum in the Control experiment is stronger than that in the Control-5N experiment due to the meridional SST gradient being larger in the former than in the latter. Precipitation differences between the two experiments can also be noticed in the midlatitudes, especially in the Northern Hemisphere.

The wave characteristics in the Control-5N experiment are shown in Fig. 8. Because of the northward shift of maximum SSTs, the SST forcing is no longer symmetric about the equator, thus tropical wave behaviors are different from those in the Control experiment. Though some waves are still pronounced such as the eastward Kelvin wave as compared to those in the Control experiment, the significant regions of both symmetric and antisymmetric components about the equator shrink significantly in which dominant waves are suppressed. However, the depths of significant waves such as Kelvin are similar and around 25 m, since the model is the same and the coupling between dynamics and physics are not changed, which is also pointed out by Lin (2006). The spectral signature of the MJO is not represented here. Previous studies showed that the strongest MJO occurs in winter and spring, while it is weak in summer (Li and Wang, 1994). Thus the weak MJO may be related to the northward migration of the warmest SST. But, the eastward antisymmetric wave is more significant in the Control-5N experiment than in the Control experiment; its spectral peak has periods of about 20

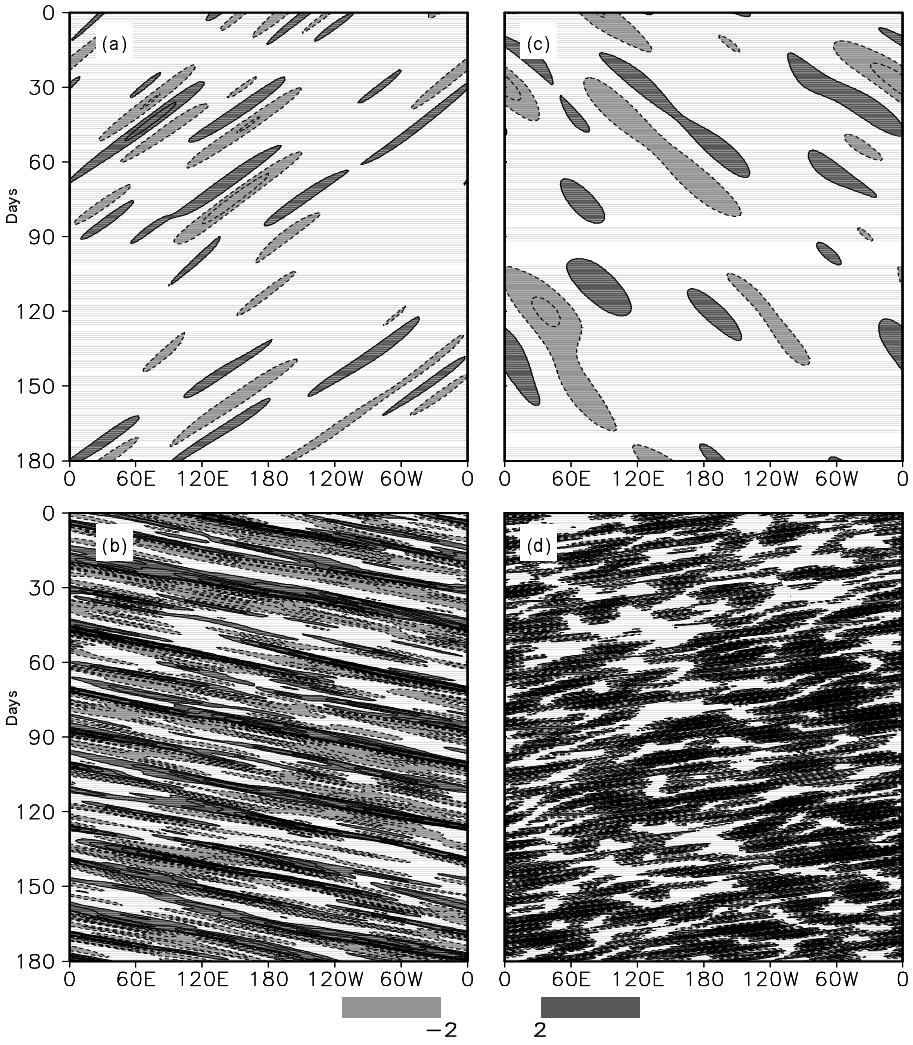

Fig. 7. Time-longitude sections of the simulated precipitation anomalies for different wave-filtered bands of (a) the $n = 1$ ER wave, (b) the Kelvin wave, (c) the MJO, and (d) the $n = 1$ WIG wave for 180 days and averaged for latitudes from 10°S to 10°N. The zero contours have been omitted. Dark shading is for positive anomalies and light shading for negative anomalies. The values have been scaled by 10^{-5} kg m^{-2} s^{-1}.

days at wavenumbers 1–3 (Fig. 8b), which cannot be classified as any waves in the shallow water theory, implying that the eastward low-frequency antisymmetric waves are more significant in summer than in winter and spring.

The total variance of all wave modes from planetary to synoptic scales is maximized off the equator immediately south of 5°N (not shown). As compared to the Control experiment, the total variance amount is reduced, indicating a weakened strength of tropical waves, which is accordant with the power spectrum distribution (see Fig. 8). The zonal mean variances of simulated precipitation variances from the Control-5N experiment for each of different wavenumber-frequency bands are presented in Fig. 9. It is obvious that all the waves become weak, while the symmetric ones are weakened more significantly. Note that the maximum values of the Kelvin wave, WIG and $n = 1$ ER wave are only about one third of those in the Control experiment, and the strength of $n = 1$ ER is even comparable to that of EIG. However, the influences of the off-equatorial maximum SSTs on the meridional distributions of tropical waves are different for different waves. The significantly influenced waves are the Kelvin and WIG waves, with the active regions of these two waves becoming wider from about 2° in Control experiment to 4° in Control-5N experiment. However, the EIG as well as the MRG waves almost keep the same region, suggesting that the SST distributions have more influences on distributions of symmetric waves than

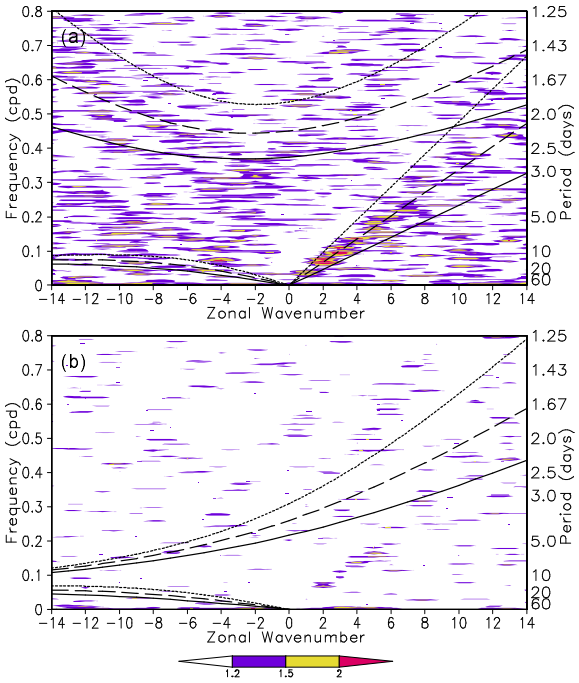

Fig. 8. Same as Fig. 5, but for the Control-5N experiment.

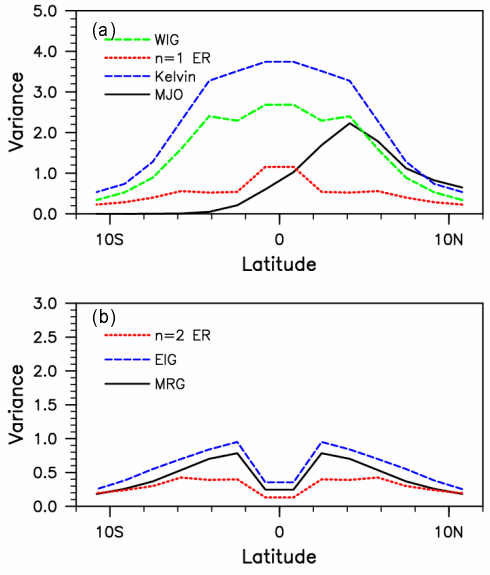

Fig. 9. Same as Fig. 6, but for the Control-5N experiment.

on those of antisymmetric waves, which is in agreement with the observation that shows little seasonal variation (Wheeler and Kiladis, 1999). The distribution of $n = 1$ ER is also not influenced by the SST variation.

Though the spectral signature of the MJO is not significant (Fig. 8a) and its maximum variance is also weakened, the reduction is quite small compared with Kelvin and WIG waves. Note that the MJO magnitude is almost the same as the WIG wave in the Control-5N experiment, while their difference are quite large in the Control experiment (Figs. 6a and 9a). Actually, the significant impact of SST on MJO is manifested in terms of the maximum variance location. The maximum variance of MJO occurs in the region where maximum SSTs are located. Therefore, the seasonal variations of MJO may be caused by the seasonal variations of SST (Li and Wang, 1994; Raymond, 2001).

6. Response to the Zhang-McFarlane convective scheme

In addition to the impact of the SST distributions, the simulated precipitation and corresponding tropical waves are closely related to the convective parameterization used in the model. Hess et al. (1993) had compared the influences between the Manabe moist convective adjustment scheme (Manabe et al., 1965) and the Kuo convective parameterization when they explored the formation mechanism of the ITCZ. Their studies showed that the precipitation distributions are very sensitive to the parameterization scheme. Our SAMIL model adopts the Manabe moist convective adjustment scheme (Manabe et al., 1965), while the NCAR CCSM CAM2 model uses the ZM mass flux scheme (Zhang and McFarlane, 1995). The ZM scheme is based on a plume ensemble approach in which an ensemble of convective-scale updrafts and downdrafts is assumed to exist when the atmosphere is conditionally unstable in the lower troposphere, while in the Manabe scheme the moist convective condensation takes place only when the lapse rate tends to become supermoist-adiabatic and the relative humidity tends to exceed 100 percent (Manabe et al., 1965). Significant differences are found in the simulated precipitation distributions between these two models. The precipitation from the SAMIL model is more confined to the equator (Fig. 4), while the rainfall strength from the NCAR CCSM CAM2 model is weaker than that from the SAMIL model, with two weak peaks on the sides of the equator (not shown). Moreover, the rainfall maxima in the CAM2 exhibit a broader width than in the SAMIL model. In this study, the ZM scheme is introduced into the SAMIL model to show the impacts of different convective schemes on the tropical waves in one model by comparing the differences of the Control and Control-ZM experiments. As the simulated basic states in the Control and Control-ZM experiments are very similar (not shown), their differences may represent the direct impacts of these two con-

vection schemes. Though the tropical precipitation is dominated by the convective processes, the convection can interact with the dynamics and with other physical processes that are also important to simulate the wave characteristics. To further examine such an impact of the convective parameterization scheme on tropical waves, we compare the simulated results between the NCAR-Control and Control-ZM experiments.

Similar to Fig. 5, the power spectrum ratios of tropical waves to the background power in the wavenumber-frequency domain for the NCAR-Control and Control-ZM experiments are shown in Fig. 10. Several primary waves can be seen from these two experiments such as significant Kelvin and ER waves. The focus here is on their principal differences. For the Kelvin wave, in the NCAR-Control experiment the wave equivalent depth is above 50 m with a high frequency of above 0.2 cycles per day (cpd), while in the Control-ZM experiment the equivalent depth is within 12–50 m with a low frequency of below 0.2 cpd and is similar to that in the Control experiment (Fig. 5). According to the study of Frierson (2007), the enhanced, slower propagating Kelvin waves occur in the cases with some large-scale precipitation. The large-scale precipitation in the NCAR-Control experiment in the tropics is very weak, while in the Control experiment, the large-scale precipitation is about one-third of the total precipitation (not shown). The phase speed is also associated with the vertical mode of the waves (Lau and Peng, 1987). Thus the faster Kelvin wave in the NCAR-Control experiment may be associated with the large-scale condensation simulations in the model. Note also that the significant distributions of both symmetric and antisymmetric waves in the Control-ZM experiment (Figs. 10c and 10d) are similar to those in the Control experiment (Fig. 5). The large-scale condensation scheme is very sensitive to the moisture, which may be related with the moisture control of deep convection for simulating the convectively coupled equatorial waves. Therefore, the phase speed of the tropical waves may be associated with the moisture control of convection and the large-scale condensation scheme used in the model. For the MJO signal, in the NCAR-Control experiment both symmetric and antisymmetric components within wavenumbers 4–6 are significant, while in the Control-ZM experiment the symmetric component is pronounced within wavenumbers 2–5, while the antisymmetric component is very weak. On the other hand, the antisymmetric waves such as the $n = 2$ ER wave and MRG are more evident in the NCAR-Control experiment, which might relate with the basic state simulation in the model with the double ITCZ. Lee et al. (2003) also showed that the strength of convection trigger in the model can significantly change the ITCZ structure, and hence the wave activities in the tropics from their AP experiment.

For the distribution of total variance (not shown), the NCAR-Control signals occupy a broad latitudinal band from 10°S to 10°N with a uniform rainfall distributing zonally, while the Control-ZM signals concentrate on a relatively narrow latitudinal band between 5°S to 5°N with some main centers of convective variance. On the other hand, compared to that of the Control experiment, the total variance of the Control-ZM experiment is of a smaller magnitude though their significances are similar. Since the dynamic and other physical processes are the same, this may represent the direct influence of the details of the convective schemes, such as the convection closure (Zhang and Mu, 2005) and the relative humidity criterion for convection trigger (Wang and Schlesinger, 1999; Lee et al., 2003; Lin et al., 2008). With a simplified model Frierson (2007) pointed out that the wave amplitude decreases dramatically with increasing relaxation time. In the ZM scheme, the relaxation time is 2 h (Zhang and Mu, 2005), while in the Manabe adjustment scheme there is no relaxation time. This may provide one explanation for why the ZM parameterization scheme is not conducive to the tropical wave activities.

Figure 11 displays the zonal mean distributions of simulated precipitation variances from the NCAR-Control and Control-ZM experiments for each of different wavenumber-frequency bands. Only dominant waves are discussed here. Though the waves are significant compared with the background signals (Fig. 10), the variances of all waves are weakened in the NCAR-Control and Control-ZM experiments when compared with the Control experiment. Other AP experiments with different models also simulate similar results as in our study (e.g., Wang and Schlesinger, 1999; Lee et al., 2003). The general conclusion is that the moist convection adjustment scheme produces the largest intraseasonal variability and the Arakawa-Schubert scheme (1974) produces the weakest. Since the ZM scheme here is a mass flux scheme inspired by the convective parameterization of Arakawa and Schubert, it is understandable that the wave variances are reduced when the ZM scheme is used in the NCAR-Control and Control-ZM experiments. One possible reason why the ZM convection scheme fails to simulate the tropical intraseasonal variability and MJO is the use of convective available potential energy as closure to determine the amount of convection in the atmosphere. In this scheme, the convection occurs almost at all times in the tropics, leading to weak temporal variability. However, the relative humidity threshold for convection trigger may have larger impact on the in-

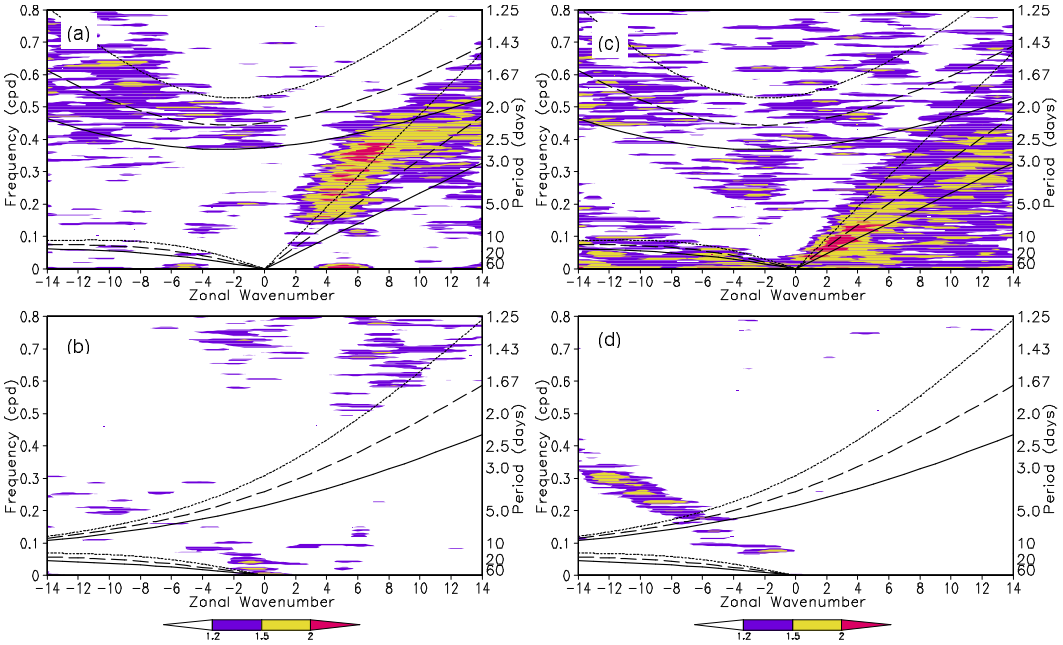

Fig. 10. Same as Fig. 5, but (a), (b) for the NCAR-Control experiment (left panels) and (c), (d) for the Control-ZM experiment (right panels).

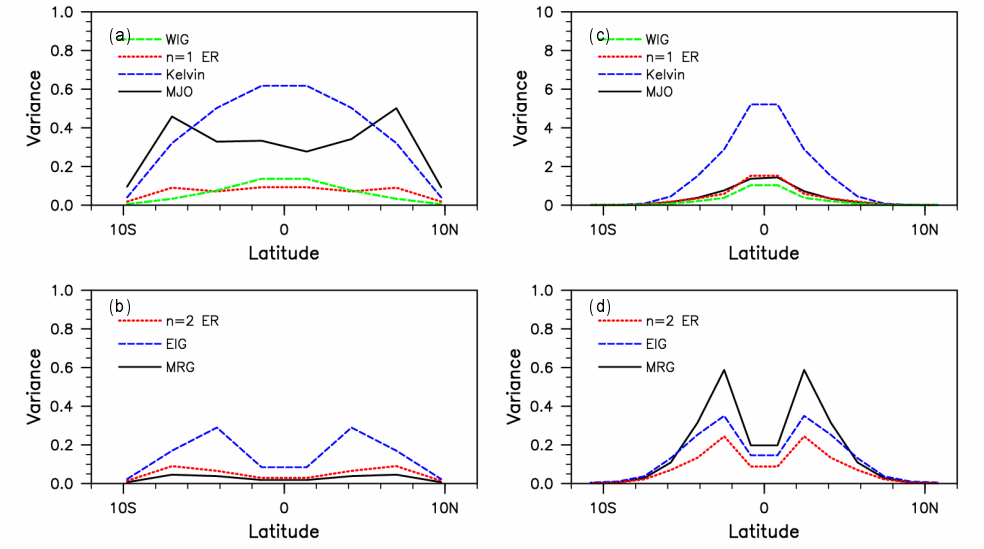

Fig. 11. Same as Fig. 6 but (a), (b) for the NCAR-Control experiment (left panels), and (c), (d) for the Control-ZM experiment (right panels).

tensity of the simulated MJO signal in precipitation (Zhang and Mu, 2005; Lin et al., 2008). For the variance of individual wave, in the Control-ZM experiment the Kelvin wave signal is the strongest (Fig. 11c), next is the $n = 1$ ER wave, while the MJO signal is comparable to that of the $n = 1$ ER wave. This is consistent with that in the Control experiment. However, the WIG becomes the weakest among the symmetric waves while it has the same value with the Kelvin in the Control experiment, which may imply that the ZM scheme is not suitable for the WIG. Further in the NCAR-Control experiment, the Kelvin wave is still the strongest wave though the magnitude is significantly weakened. The next one is the MJO. Such a weakened Kelvin wave may be due to the fact that the significant wavenumber-frequency domain of the Kelvin wave is not included into the defined filtering region (Fig. 10a). Each wave in the NCAR-Control exper-

iment has a broader width than in experiments with the SAMIL model, which may imply that the simulated basic state is important to the meridional distributions of the waves. Though the zonal resolution of SAMIL is same as that of NCAR CAM2, its meridional resolution is higher. Some studies with rhomboidal truncated models (Hayashi and Golder, 1986) also showed that the model's resolution may affect the simulations, though the model resolution may be not the direct cause for the differences in the waves (Slingo et al., 1996). This may explain why the waves are confined in the equator in the experiments with SAMIL. Compared with the Control experiment, the strengths of both the Kelvin and $n = 1$ ER waves are weakened, especially the peaks at the equator. The prominent characteristic of the MJO in the NCAR-Control is that the maximum location is not at the equator, but off the equator with two peaks. Note also that though the MJO magnitude in the Control-ZM experiment is reduced compared to that in the Control experiment, the meridional distributions are quite similar, which suggests that the convection parameterization scheme as well as the physical processes linking the convection with large-scale disturbances may have different impacts on the strength and distribution of the MJO.

7. Conclusions

In this study, results from several aqua-planet experiments based on the SAMIL model developed at LASG/IAP, which are forced with symmetric equinoctial insolation and prescribed idealized-SST distribution, are analyzed to reveal the influences of SST distribution and convective parameterization on the tropical wavenumber-frequency characteristics. Based on the simulated total precipitation, the space-time spectral analysis is applied to isolate dominant modes of convectively coupled equatorial waves including the Kelvin, ER, MRG, EIG and WIG waves, examining the power spectrum and variance distributions of these waves. Also examined are the behaviors of the MJO.

The basic simulation of the zonal mean climate such as precipitation, winds and potential temperature in the Control experiment shows that both the distribution and the magnitude resemble those in the observed climate mainly due to the full physics being retained, though the underlying basis of the model is simplified and covered only by oceans. The simulated circulation and precipitation are almost symmetric about the equator and distributed evenly in the zonal direction, which are accordant with zonally symmetric SSTs and radiative forcings prescribed in the model. However, since there are no asymmetries of land and sea distribution, and the eddy transport is very weak, thus the zonal wind is too strong and rather confined in latitudinal extend.

Both the symmetric and antisymmetric waves can be reproduced in the Control experiment, with Kelvin and $n = 1$ ER waves being especially prominent, which are consistent with the observations and theoretical dispersion curves. The equivalent depth of each wave is around 25 m, which is also observed in the observational rainfall data. The meridional distributions of the simulated precipitation variance in the Control experiment show that the maximum variance occurs over the equatorial region. The Kelvin wave is the most significant among these waves, and its variance can explain more than 10% of the variance of all the scales. The variance of the WIG wave is comparable to that of the Kelvin wave. However, the MJO has the variance of a similar magnitude compared to the $n = 1$ ER wave, although the MJO spectrum is not significant for wavenumbers 1–2, but quite significant for wavenumbers 4–10. Actually, other AP experiments and full AGCM with prescribed orography and observed SST also produce weak MJO signals. This illustrates that the simplified AP model can be used to investigate the dynamics and physical parameterization in AGCMs and diagnose the complex AGCM with the theoretical results.

The comparison results of the Control-5N and Control experiments show that the tropical wave activities are very sensitive to the SST distribution. The only difference for these two experiments in the SST distribution is that the maximum moves northward to 5°N in the Control-5N experiment, which can be used to mimic the summer situation. Since the SSTs are not symmetric about the equator, both symmetric and antisymmetric waves in the Control-5N experiment are much weaker than those in the Control experiment. The eastward Kelvin wave is still one of the most significant waves, but its variance decreases remarkably with a broader meridional extent of the variance. A similar feature occurs in the WIG wave. Although the MJO variance also weakens, its maximum is comparable to those of the Kelvin and WIG waves in the Control-5N experiment. Importantly, the MJO maximum variance also moves to around 5°N. These suggest that the significant impact of SST on MJO is manifested in terms of the maximum variance location. Therefore, the seasonal variations of MJO may be at least partly caused by the seasonal variations of SST.

Almost all tropical waves in the NCAR-Control and Control-ZM experiments are weakened, suggesting that the ZM parameterization scheme is not favorable for the tropical wave activities. The wave variances in the NCAR-Control experiment occupy a broad lat-

itudinal band from 10°S to 10°N, while the Control-ZM signals concentrate on a relatively narrow latitudinal band between 5°S to 5°N, which may imply that the simulated basic state is important to the meridional distributions of the waves. The higher frequency of the Kelvin wave in the NCAR-Control experiment may be associated with convection indirectly, while the $n = 1$ ER wave may be more sensitive to the convection schemes.

In the NCAR-Control experiment, the strength of the MJO is significantly weakened, with two variance maxima off the equator, which is significantly different from the distribution in the Control experiment. However, in the Control-ZM experiment the MJO signal is comparable to that of the $n = 1$ ER wave, and the distribution is similar to that in the Control experiment, which suggests that the parameterization scheme may have less direct impact on the MJO distribution than the dynamics and other processes such as SST or air-sea interactions. This may be conflicted with other studies in which the modification of convective scheme can lead to the improvement of the MJO simulation (e.g., Zhang and Mu, 2005; Liu et al., 2005). However, many other studies also show that the MJO is strongly tied to the surface frictional convergence (Maloney, 2002), and may also be related to other aspects such as the low-frequency external coupling and the basic state simulation (Ajayamohan and Goswami, 2007). However, it is implied that the strength and distribution of the MJO may have different mechanisms, and this is also an indication of the difficulty to simulate the MJO properly in the AGCM, and the MJO should receive more attention because of its importance in climate simulation and its role in model performance. In addition, the results may be model-dependent, and much analysis needs to be done on the simulations to understand the mechanisms and the feedbacks between the convection and dynamics.

Acknowledgements. We would like to thank the two anonymous reviewers for their valuable comments. The authors thank the NCAR CCSM modeling group for providing the data for analysis through APE Project, the Program for Climate Model Diagnosis and Intercomparson (PCMDI) for collecting and archiving the model data. This research was supported by the International Partnership Creative Group of Chinese Academy of Sciences entitled "Climate System Model Development and Application Studies" and National Basic Research Program of China (Grant Nos. 2006CB403600 and 2005CB422004).

REFERENCES

Ajayamohan, R. S., and B. N. Goswami, 2007: Dependence of simulation of boreal summer tropical intraseasonal oscillations on the simulation of seasonal mean. *J. Atmos. Sci.*, **64**, 460–478.

Arakawa, A., and W. H. Schubert, 1974: Interaction of a cumulus cloud ensemble with the large-scale environment. Part I. *J. Atmos. Sci.*, **31**, 674–701.

Dong, M., C. D. Zhang, and J. H. He, 2006: A simulation study of the influence of external forcing on the tropical intraseasonal oscillation. *Chinese J. Atmos. Sci.*, **30**(3), 413–422. (in Chinese)

Frierson, D., 2007: Convectively coupled Kelvin waves in an idealized moist general circulation model. *J. Atmos. Sci.*, **64**, 2076–2090.

Gates, W. L., 1992: AMIP: The atmospheric intercomparison project. *Bull. Amer. Meteor. Soc.*, **73**, 1962–1970.

Gill, A. E., 1980: Some simple solutions for heat-induced tropical circulation. *Quart. J. Roy. Meteor. Soc.*, **106**, 447–462.

Hayashi, Y., 1982: Space-time spectral analysis and its applications to atmospheric waves. *J. Meteor. Soc. Japan*, **60**, 156–171.

Hayashi, Y., and D. G. Golder, 1986: Tropical intraseasonal oscillations appearing in a GFDL general circulation model and FGGE data. Part I: Phase propagation. *J. Atmos. Sci.*, **43**, 3058–3067.

Held, I. M., and M. J. Suarez, 1994: A proposal for the intercomparison of the dynamical cores of atmospheric general circulation models. *Bull. Amer. Meteor. Soc.*, **75**, 1825–1830.

Hess, P. G., D. S. Battisi, and J. R. Rasch, 1993: Maintenance of the intertropical convergence zones and the large-scale tropical circulation on a water-covered earth. *J. Atmos. Sci.*, **50**, 691–713.

Ichikawa, H., and T. Yasunari, 2006: Time-space characteristics of diurnal rainfall over Borneo and surrounding oceans as observed by TRMM-PR. *J. Climate*, **19**, 1238–1260.

Lau, K. M., and L. Peng, 1987: Origin of low-frequency (intraseasonal) oscillations in the tropical atmosphere. *J. Atmos. Sci.*, **44**, 950–972.

Lee, M.-I., I.-S. Kang, and B. E. Mapes, 2003: Impacts of cumulus convection parameterization on aqua-planet AGCM simulations of tropical intraseasonal variability. *J. Meteor. Soc. Japan*, **81**, 963–992.

Li, C. Y., X. L. Jia, and M. Dong, 2006: Numerical simulation and comparison study of the atmospheric intraseasonal oscillation. *Acta Meteorologica Sinica*, **64**, 412–419. (in Chinese)

Li, T., and B. Wang, 1994: The influence of sea surface temperature on the tropical intraseasonal oscillation: a numerical study. *Mon Wea. Rev.*, **122**, 2349–2362.

Li, W., R. C. Yu, and H. L. Liu, 2002: Responses of Madden-Julian oscillation in the Community Climate Model to different SST forcing. *Journal of Ocean, University of Qingdao*, **32**(1), 9–17. (in Chinese)

Lin, J. L., and Coauthors, 2006: Tropical intraseasonal variability in 14 IPCC AR4 climate models. Part I: Convective signals. *J. Climate*, **19**, 2665–2690.

Lin, J.-L., M.-I. Lee, D. Kim, and I.-S. Kang, D. W. Frierson, 2008: Impacts of convective parameterization and moisture convective trigger on AGCM-simulated convectively coupled equatorial waves. *J. Climate*, **21**, 883–909.

Lindzen, R. S., 1967: Planetary waves on beta planes. *Mon. Wea. Rev.*, **95**, 441–451.

Liu, P., B. Wang, K. R. Sperber, T. Li, and G. A. Meehl, 2005: MJO in the NCAR CAM2 with the Tiedtke convective scheme. *J. Climate*, **18**, 3007–3020.

Louis, J. F., 1979: A parametric model of vertical eddy fluxes in the atmosphere. *Bound.-Layer Meteor.*, **17**, 187–202.

Madden, R. A., and P. R. Julian, 1971: Detection of a 40–50 day oscillation in the zonal wind in the tropical Pacific. *J. Atmos. Sci.*, **28**, 702–708.

Madden, R. A., and P. R. Julian, 1994: Observations of the 40–50 day tropical ascillation—A review. *Mon. Wea. Rev.*, **122**, 814–837.

Maloney, E. D., 2002: An intraseasonal oscillation composite life cycle in the NCAR CCM3.6 with modified convection. *J. Climate*, **15**, 964–982.

Maloney, E. D., and D. L. Hartmann, 2001: The sensitive of intraseasonal variability in the NCAR CCM3 to the changes in the convection parameterization. *J. Climate*, **14**, 2015–2034.

Manabe, S., J. Smagorinsky, and R. F. Strickler, 1965: Simulated climatology of a general circulation model with a hydrologic cycle. *Mon. Wea. Rev.*, **93**, 769–799.

Matsuno, T., 1966: Quasi-geostrophic motions in the equatorial area. *J. Meteor. Soc. Japan*, **44**, 25–43.

Neale, R. B., and B. J. Hoskins, 2001a: A standard test for AGCMs including their physical parameterizations: I: The proposal. *Atmospheric Science Letters*, **1**, 101–107.

Neale, R. B., and B. J. Hoskins, 2001b: A standard test for AGCMs including their physical parameterizations: II: Results for the Met Office model. *Atmospheric Science Letters*, **1**, 108–114.

Numaguti, A., 1995: Dynamics and energy balance of the Hadley circulation and the tropical precipitation zones. Part II: Sensitivity to meridional SST distribution. *J. Atmos. Sci.*, **52**, 1128–1141.

Raymond, D. J., 2001: A new model of the Madden-Julian oscillation. *J. Atmos. Sci.*, **58**, 2807–2819.

Shao, H., Y. F. Qian, and Q. Q. Wang, 1998: The effects of the diurnal variation of solar radiation on climate modeling of R15L9. *Plateau Meteorology*, **17**, 158–169. (in Chinese)

Shi, G. Y., 1981: An accurate calculation and representation of the infrared transmission function of the atmospheric constituents. Ph. D dissertation, Tohoku University of Japan, 191pp.

Slingo, J. M., 1987: The development and verification of a cloud prediction scheme for the ECMWF model. *Quart. J. Roy. Meteor. Soc.*, **113**, 899–927.

Slingo, J. M., and Coauthors, 1996: Intraseasonal oscillation in 15 atmospheric general circulation models: results from an AMIP diagnostic subprojects. *Climate Dyn.*, **12**, 325–357.

Swinbank, R., T. N. Palmer, and M. K. Davey, 1988: Numerical simulations of the Madden and Julian oscillation. *J. Atmos. Sci.*, **45**, 774–788.

Waliser, D. E., K. M. Lau, and J. H. Kim, 1999: The influence of coupled sea surface temperatures on the Madden-Julian Oscillation: A model perturbation experiment. *J. Atmos. Sci.*, **56**, 333–358.

Wang, W., and M. E. Schlesinger, 1999: The dependence on convective parameterization of the tropical intraseasonal oscillation simulated by the UIUC 11-layer atmospheric GCM. *J. Climate*, **12**, 1423–1457.

Wang, Z. Z., G. X. Wu, T. W. Wu, and R. C. Yu, 2004: Simulation of Asian monsoon seasonal variations with climate model R42L9/LASG. *Adv. Atmos. Sci.*, **21**, 879–889.

Wheeler, M., and G. N. Kiladis, 1999: Convectively-coupled equatorial waves: Analysis of clouds and temperature in the wavenumber-frequency domain. *J. Atmos. Sci.*, **56**, 374–399.

Wu, G. X., P. Liu, and Y. M. Liu, 2002: Impacts of the sea surface temperature anomally in the Indian Ocean on the subtropical anticyclone over the western Pacific—two-stage thermal adaptation in the atmosphere. *Acta Meteorologica Sinica*, **58**, 513–521. (in Chinese)

Wu, G. X., H. Liu, Y. Zhao, and W. Li, 1996: A nine-layer atmospheric general circulation model and its performance. *Adv. Atmos. Sci.*, **13**, 1–18.

Yang, G., B. Hoskins, and J. Slingo, 2003: Convectively coupled equatorial waves: A new methodology for identifying wave structures in observational data. *J. Atmos. Sci.*, **60**, 1637–1654.

Yang, X.Q., 1990: A numerical study of the low-frequency response of atmosphere to the tropical heat source. *Scientia Meteorologica Sinica*, **10**, 384–393. (in Chinese)

Zhang, G. J., and N. A. McFarlane, 1995: Sensitivity of climate simulations to the parameterization of cumulus convection in the Canadian Climate Centre General Circulation Model. *Atmos.-Ocean*, **33**, 407–446.

Zhang, G. J., and M. Mu, 2005: Simulation of the Madden-Julian Oscillation in the NCAR CCM3 using a revised Zhang-McFarlane convection parameterization scheme. *J. Climate*, **18**, 4046–4064.

Zhang, X. H., G. Y. Shi, H. Liu, and Y. Q. Yu. 2000: *IAP Global Ocean-Atmosphere-Land System Model*. Science Press, Beijing, 252pp.